Self-organization of axial polarity, inside-out layer pattern, and species-specific progenitor dynamics in human ES cell–derived neocortex

Taisuke Kadoshima[a,b,1], Hideya Sakaguchi[a,b], Tokushige Nakano[a,2], Mika Soen[a], Satoshi Ando[a,2], Mototsugu Eiraku[c], and Yoshiki Sasai[a,b,3]

[a]Laboratory of Organogenesis and Neurogenesis and [c]Four-Dimensional Tissue Analysis Unit, RIKEN Center for Developmental Biology, Kobe 650-0047, Japan; and [b]Department of Medical Embryology, Kyoto University Graduate School of Medicine, Kyoto 606-8501, Japan

Edited by Chen-Ming Fan, Carnegie Institution of Washington, Baltimore, MD, and accepted by the Editorial Board October 17, 2013 (received for review August 21, 2013)

Here, using further optimized 3D culture that allows highly selective induction and long-term growth of human ES cell (hESC)-derived cortical neuroepithelium, we demonstrate unique aspects of self-organization in human neocorticogenesis. Self-organized cortical tissue spontaneously forms a polarity along the dorsocaudal-ventrorostral axis and undergoes region-specific rolling morphogenesis that generates a semispherical structure. The neuroepithelium self-forms a multilayered structure including three neuronal zones (subplate, cortical plate, and Cajal-Retzius cell zones) and three progenitor zones (ventricular, subventricular, and intermediate zones) in the same apical-basal order as seen in the human fetal cortex in the early second trimester. In the cortical plate, late-born neurons tend to localize more basally to early-born neurons, consistent with the inside-out pattern seen in vivo. Furthermore, the outer subventricular zone contains basal progenitors that share characteristics with outer radial glia abundantly found in the human, but not mouse, fetal brain. Thus, human neocorticogenesis involves intrinsic programs that enable the emergence of complex neocortical features.

corticogenesis | stratification

The mammalian neocortex has a multilayered structure (layers I–VI) (1). The neocortex arises from the neuroepithelium (NE) of the dorsal telencephalon, which evaginates to form a semispherical brain vesicle (Fig. S1*A*) (2). The dorsocaudal side of the neocortex is flanked by the cortical hem, whereas its ventrorostral side is neighbored by the lateral ganglionic eminence (LGE; striatum anlage) and septum. Layer I [its fetal primordium is called the marginal zone (MZ); Fig. S1*B*] is qualitatively different from other layers, as this superficial-most layer is mainly composed of Reelin$^+$ Cajal-Retzius (CR) cells, which are largely derived from neighboring tissues such as the cortical hem and septum (3) (in the case of human cortex, some Reelin$^+$ cells also arise directly from neocortical NE) (4). The rest of the cortical layers are generated with the "inside-out" pattern: the deeper the layer, the earlier the neurons are born from cortical progenitors (Fig. S1*B*) (5, 6).

A detailed understanding of early human corticogenesis remains elusive because of the limited access to fetal brain tissues. We previously established a 3D culture of mouse and human ES cell (hESC) aggregates that recapitulates early steps of corticogenesis [or serum-free floating culture of embryoid body-like aggregates with quick reaggregation (SFEBq)] (7–9). This method has been also applied to human induced pluripotent stem (iPS) cell culture (10). In this self-organization culture, large domains of cortical NE self-form within a floating hESC aggregate and spontaneously develop ventricular zone (VZ), cortical plate (CP) (mostly deep-layer neurons), and MZ by culture day 40–45. This cortical NE was still immature, mimicking human corticogenesis during the first trimester (Fig. S1*C*) (7).

Here, using an optimized culture, we revealed unique self-organizing aspects of human corticogenesis. Moreover, the optimized culture generates species-specific progenitors in the outer subventricular zone (oSVZ), called outer radial glia (oRG), which are abundantly present in the human neocortex (11, 12) but rare in the mouse cortex (13, 14). Thus, an unexpectedly wide range of self-organizing events is internally programmed within the cortical NE.

Results

Intracortical Polarity in Self-Organized Cortical NE. For the improved SFEBq culture (Fig. S2 *A* and *A′*), we formed aggregates by plating 9×10^3 dissociated hESCs into each well of V-bottomed 96-well plates (15) and culture them in medium supplemented with the Rho kinase inhibitor (16) (Fig. S2*A*). Then, the aggregates were transferred to petri dishes and cultured under 40% O_2 conditions. The addition of chemically defined lipid concentrate, FBS, heparin, and a low concentration of Matrigel improved long-term maintenance of VZ progenitors, whereas the addition of a TGFβ inhibitor and a Wnt inhibitor for the first 18 d moderately promoted telencephalic differentiation.

Under these conditions, all hESC aggregates were positive for *foxg1::*Venus (marking telencephalic tissue) (2) on days 26 (Fig. 1*A* and Fig. S2*B*), and >75% of total cells (day 34) expressed *foxg1::*Venus, in contrast to the previous culture (Fig. 1*B* and Fig. S2*C*). The *foxg1::*Venus$^+$ NE contained epithelial domes with a ventricle-like cavity inside (Fig. 1*C*; day 42). These thick epithelia had a cell-dense VZ positive for Pax6 and Sox2 on the luminal side (Fig. 1 *D* and *E*), whereas pH3$^+$ progenitors under mitosis were found exclusively in its innermost part (Fig. 1*F*), as seen in vivo. TuJ1$^+$ neurons occupied the zone outside of the VZ (CP; Fig. 1*G*), and expressed markers of early CP neurons such

Significance

Using 3D culture of human ES cells, we show new self-organizing aspects of human corticogenesis: spontaneous development of intracortical polarity, curving morphology, and complex zone separations. Moreover, this culture generates species-specific progenitors, outer radial glia, which are abundantly present in the human, but not mouse, neocortex. Our study suggests an unexpectedly wide range of self-organizing events that are driven by internal programs in human neocortex development.

Author contributions: T.K. and Y.S. designed research; T.K., H.S., T.N., M.S., S.A., and M.E. performed research; T.K. and Y.S. analyzed data; and T.K. and Y.S. wrote the paper.

The authors declare no conflict of interest.

This article is a PNAS Direct Submission. C.-M.F. is a guest editor invited by the Editorial Board.

[1]Present address: Faculty of Exploratory Pharmacology, Asubio Pharma Co., Ltd., Kobe 650-0047, Japan.

[2]Present address: Environmental Health Science Laboratory, Sumitomo Chemical Co., Ltd., Osaka 554-8558, Japan.

[3]To whom correspondence should be addressed. E-mail: yoshikisasai@cdb.riken.jp.

This article contains supporting information online at www.pnas.org/lookup/suppl/doi:10.1073/pnas.1315710110/-/DCSupplemental.

as Ctip2 and Tbr1 (1, 2) (Fig. 1*H* and Fig. S2*D*). The neuronal zone also contained Reelin^{+} cells (Fig. 1*I*), and a Laminin-rich zone near the surface (Fig. 1*J*) (4). Thus, self-organizing lamination occurs in this hESC-derived cortical NE.

Interestingly, the cortical NE frequently had an axial polarity. Expression of Coup-TF1 in the VZ (Fig. 1*K*, red), which forms a dorsocaudal-to-rostroventral gradient in the fetal brain (Fig. S2 *E* and *F*), was stronger on one side of the hESC-derived cortical NE, whereas the ventrorostral marker Sp8 was expressed in the reverse pattern (Fig. 1*K*, white). Consistent with this idea, Lhx2 expression (forming a dorsal-to-ventral gradient of signal intensity in vivo) was also strong on the same side with Coup-TF1 (Fig. 1*L* and Fig. S2*G*). The reverse gradient pattern of Coup-TF1 and Sp8 was already observed on day 35. In the mouse embryo, the dorsocaudal cortical area is flanked by the cortical hem (Fig. S2 *H–J*), which later gives rise to the fimbria of the hippocampus. Consistent with this, the cortical hem markers Otx2 and Zic1 were expressed in the tissue flanking the cortical NE on the side with strong Coup-TF1 expression (Fig. 1*M* and Fig. S2*K*).

These findings indicate that hESC-derived NE spontaneously acquires an intracortical dorsocaudal-ventrorostral polarity. In the embryo, FGF8 promotes rostral specification of neocortical NE (17). Interestingly, a higher level of pErk signals (working downstream of FGF signaling) was observed in the hESC-derived cortical NE on the side opposite to Coup-TF1 expression (Fig. 1*N*). Conversely, treatment with exogenous FGF8 caused broad expression of Sp8 at the expense of Coup-TF1 expression (Fig. 1 *O* and *P* and Fig. S2*L*), suggesting an active role of FGF-MAPK signaling in the rostral specification.

Polarized Curving Morphogenesis of Self-Organized Cortical NE. Foxg1 was first detected in hESC-derived NE around days 18–20. The apical side (aPKC^{+}) of the NE was located on the surface of the aggregate (Fig. 2*A*, *Lower*). On day 21, the NE structure started to break into several large domains (Fig. 2*A*), and subsequently became apically concave (Fig. 2 *B–D* and Fig. S3*A*, *Upper*).

Each cortical NE domain had an asymmetrically curved structure. One end of the NE was characterized by an epithelium with a rolling shape (Fig. 2 *B–D*, arrows), whereas the other side had a blunt end. Active myosin (indicated by phosho-myosin light chain 2) was highly enriched throughout the apical surface of the cortical domain (Fig. 2*C*). In live imaging, the rolling side of the cortical domain approached the other end and eventually contacted it (Fig. 2 *E* and *F* and Movie S1). The main body of NE moved around in the same direction with the rolling end (Fig. 2 *E–H*), and generated a semispherical structure with a lumen inside (Fig. 2*I* and Fig. S3*A*, *Lower*).

The rolling morphogenesis of the cortical domain was attenuated by ROCK inhibitor treatment (days 26–30) (Fig. 2 *J–L*), which inhibits the Rho-ROCK-myosin pathway necessary for causing apical constriction. The rolling side of NE expressed markers for the dorsocaudal side (Otx2 and CoupTF1; Fig. 2 *M* and *N*), indicating that the rolling end corresponded to the dorsocaudal side.

When the NE was partially ventralized (18, 19) by a moderate level of Hedgehog agonist (30 nM smoothened agonist or SAG for days 15–21), a substantial portion of *foxg1*::Venus^{+} NE expressed Gsh2, a marker for LGE (20) (Fig. 2*O*, arrowhead, and Fig. S3*B*). A mass of GAD65^{+} GABAergic neurons was generated underneath this LGE NE, as seen in vivo (19) (Fig. 2*P*, red), whereas the rest of the telencephalic NE was largely positive for the cortical NE marker Pax6 (Fig. 2*Q*). Higher concentrations of SAG induced the medial ganglionic eminence (MGE) marker Nkx2.1 at the cost of Pax6 and Gsh2 expression (Fig. S3 *B* and *C*). Importantly, the NE treated with moderate Hedgehog signals frequently exhibited continuous formation of cortical

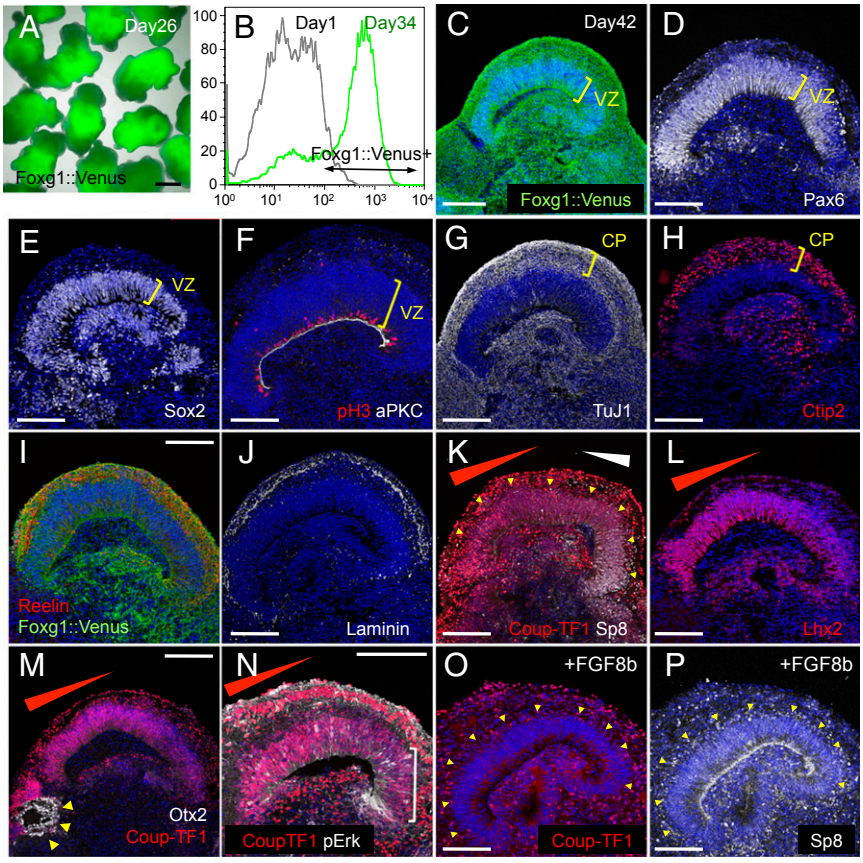

Fig. 1. Axial polarity in cortical NE self-organizes from hESCs. (*A*) hESC aggregates containing cortical NE visualized with *foxg1*::Venus on day 26. (*B*) Representative FACS analysis for *foxg1*::Venus^{+} populations. Gray, control (day 1 culture); green, day 34 culture under the new conditions. (*C–J*) Immunostaining of semispherical cortical structures self-formed from *foxg1::venus* hESCs. VZ, ventricular zone; CP, cortical plate. (*K–N*) Self-formation of axial polarity seen in hESC-derived cortical NE. Cortical hem-like tissues (Otx2^{+}; *M*) were located in the flanking region of cortical NE on the side strong for the dorsocaudal markers Coup-TF1 (*K*) and Lhx2. A higher level of pErk signals (bracket) was observed on the side opposite to Coup-TF1 expression (*N*). Gradient and polarity of expression are indicated by triangles. Arrowhead, VZ (note that the gradients of marker expression are seen in the VZ). (*O* and *P*) Fgf8 treatment suppressed CoupTF1 and expanded the expression of the ventrorostral marker Sp8. (Scale bars, 1 mm in *A*; 200 μm in *C–P*.) Nuclear counter staining (blue), DAPI.

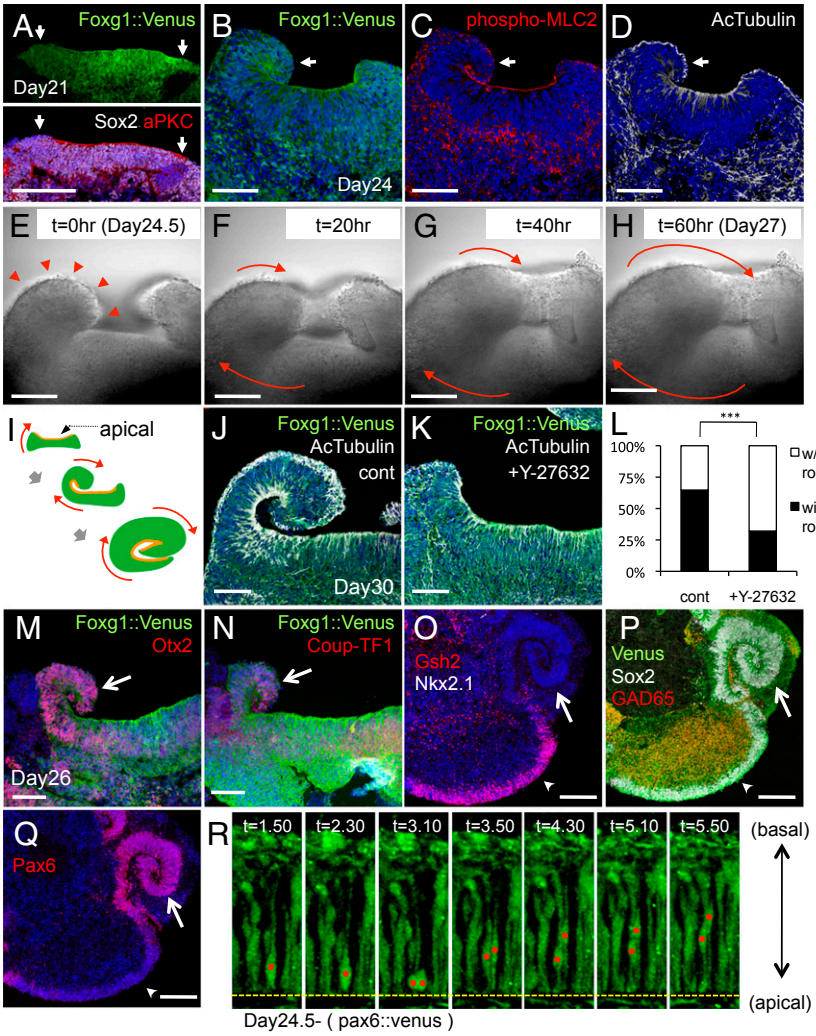

Fig. 2. Asymmetric rounding morphogenesis in self-organized cortical NE. (*A–I*) Asymmetric progression of rounding morphogenesis of hESC-derived cortical NE. Arrows, boundary of a cortical NE domain in *A* and rolling epithelium in *B–D*. Red arrowheads, rolling epithelium in *E*. Red arrows, rounding movements of the NE (*F–I*). (*J–L*) Effect of the ROCK inhibitor Y-27632 on the rolling of cortical NE. (*L*) Attenuation of rolling morphogenesis with ROCK inhibitor. ***$P < 0.001$ in contingency table analysis (2×2) with Fisher's exact test. Treatment group, $n = 187$ NE domains; control group, $n = 130$. (*M* and *N*) The rolling shape was preferentially observed on the side with strong expression of Otx2 and Coup-TF1 (dorsal and caudal markers). (*O–Q*) Adjacent formation of NE structures of cortex (Pax6$^+$) and LGE (Gsh2$^+$; with GAD65$^+$ GABAergic neurons underneath) on day 35. The cortical side contacting the LGE domain was opposite to the side with strong rolling (arrow). (*R*) Interkinetic nuclear migration in the hESC-derived cortical NE on day 24 (two-photon imaging). Visualized with partial mixing of *pax6::venus* reporter hESCs with nonlabeled hESCs. Two daughter cells with both apical and basal processes were generated from an apically dividing progenitor (red dots). (Scale bars, 200 μm in *A*; 100 μm in *B–H* and *J–N*; 200 μm in *O–Q*.) Nuclear counter staining (blue), DAPI.

(Pax6$^+$)-LGE (Gsh2$^+$) domains, as seen in vivo, suggesting that our improved culture allows self-formation of pallial-subpallial structures en bloc. In this continuously extending NE, the rolling side of the cortical NE (Fig. 2 *O–Q*, arrows) was opposite to the cortex-LGE junction, consistent with the idea that the rolling and nonrolling sides represent the dorsal and ventral side of the cortical NE, respectively.

In the embryo, the developing cortex evaginates by strong rounding morphogenesis of the pallial NE, whereas the margin of the embryonic pallium is fixed to the neighboring tissues. The curvature of the embryonic NE region from the medial pallium to the dorsal part of the neocortex is particularly strong (Fig. S1*A*). It is therefore reasonable to infer that the rounding NE movement of the cortical domain in our hESC culture reflects the strong rounding of the embryonic dorsal cortex (Fig. S3*D*).

These findings demonstrate that the hESC-derived cortical NE self-develops a cortical curvature by asymmetrical rounding morphogenesis along the self-formed dorsocaudal-ventrorostral axis. Following this topological change, the apical surface of the NE becomes located inside of the cortical semispheres. In live imaging, progenitors divided at the luminal surface while they underwent interkinetic nuclear migration, as seen in the embryonic VZ (Fig. 2*R*, Movies S2 and S3, and Fig. S3*E*; cell divisions were mostly symmetrical at these stages).

Morphological Separation of Three Cortical Neuronal Zones. The optimized culture conditions allowed cortical NE to grow even beyond day 42. On day 70, the thickness of cortical NE was 200 μm or larger (Fig. 3 *A* and *A′*). The NE was morphologically stratified into the VZ, SVZ, intermediate zone (IZ), CP, and MZ (Fig. 3 *B–G* and Fig. S4 *A* and *B*). The superficial-most portion of the MZ accumulated Laminin and contained Reelin$^+$ CR cells (Fig. 3 *C* and *C′*). Beneath the MZ was mainly the CP and contained deep-layer cortical neurons expressing Tbr1 and Ctip2 (Fig. 3 *D* and *D′*). The population of Satb2$^+$ superficial-layer (21) was still relatively small (Fig. 3*E*). On the apical side, the day 70 VZ was ~100 μm thick and cell dense with Pax6$^+$ Sox2$^+$ progenitors (Fig. 3 *F* and *F′*) or radial glia (22). Basally adjacent to the VZ, a SVZ formed and contained cells positive for Tbr2 (Fig. 3*G*).

By this stage, a distinct cell-sparse zone developed between the CP and SVZ, reminiscent of the IZ in the fetal brain. Immediately beneath the CP was a layer of Calretinin$^+$ cells with massive MAP2$^+$ neurites extending into the IZ (Fig. 3 *H* and *H′* and Fig. S4 *C* and *D*). These characteristics resemble those of neurons in the subplate (23–25). Chondroitin sulfate proteoglycans (CSPGs) are enriched in the embryonic subplate and its underlying IZ (Fig. S4*F*, *Lower Right*, bracket) (26). Similarly, strong CSPG accumulation was observed in the corresponding zones in hESC-derived cortical NE (Fig. 3*H″* and Fig. S4*E*). These findings demonstrate that hESC-derived cortical NE can self-organize not only the CP and MZ but also the subplate and IZ in a correct apico-basal order. At this stage, no substantial accumulation of GAD65$^+$ interneurons in the CP or TAG1$^+$ corticofugal axons was observed (Fig. S4*G*).

By day 91, the cortical NE reached the thickness of 300–350 μm but still contained well-developed VZ (Fig. 3 *I–K* and Fig. S4 *H* and *I*). The CP also became much thicker (~150 μm; Fig. 3*I*), and contained a number of superficial-layer neurons (Satb2$^+$ and Brn2$^+$) in addition to Tbr1$^+$ and Ctip2$^+$ deep-layer neurons (Fig. 3 *L–N* and Fig. S4*J*). The zone of subplate neurons (Calretinin$^+$) mainly localized beneath the CP (Fig. 3*O*).

The morphological zone separation seen in these late cultures (summarized in Fig. 3*P*) mimics the histology of the human fetal neocortex during early second-trimester stages (25, 27). Moreover, within the hESC-derived CP, superficial-layer neurons (Satb2$^+$ and Brn2$^+$ cells) preferentially localized more superficially to deep-layer neurons (Tbr1$^+$ and Ctip2$^+$ cells) (Fig. 4 *A–H*). Furthermore, when 1-d pulse labeling was done with 5-ethynyl-2′-deoxyuridine (EdU) on day 50 and then with BrdU on day 70, EdU- and BrdU-labeled cells were preferentially located on the deep and superficial sides of the day 91 CP, respectively (Fig. 4 *I–L*). These findings indicate a biased tendency in the localization of neurons reminiscent of the inside-out pattern during fetal corticogenesis (5, 6), in which late-born CP neurons are located outside and early-born CP neurons are inside. Consistent with this idea, on day 112, the mature cortical neuron marker CaMKIIα was preferentially seen in the apical two-thirds portion of the hESC-derived CP, which predominantly expressed Tbr1 and less Satb2 (Fig. 4 *M–O* and Fig. S4*K*). Indeed, at the cellular level, the majority of these CaMKII neurons coexpressed Tbr1 but not Satb2 (Fig. S4 *L* and *M*; Fig. 4*P* for summary).

Appearance of Human-Specific Basal Progenitors in the oSVZ. Previous in vivo studies have reported preferential nonvertical division of apical cortical progenitors at an advanced stage, when many of them produce basal progenitors through asymmetrical divisions (28, 29). In our culture, proliferating apical progenitors on day 70 preferentially divided with a "vertical" cleavage plane (60–90°; Fig. 5 *A–C*), causing segregation of daughter cells parallel to the apical surface. In contrast, on day 91, proliferating progenitors (phospho-Vimentin$^+$) showed a higher frequency of nonvertical divisions (0–60°) (Fig. 5 *D–F*).

Both on days 70 and 91, the SVZ contained a number of Tbr2$^+$ Sox2$^-$ Pax6$^-$ intermediate progenitors (Fig. 3 *G* and *M*). Interestingly, on day 91, the outer portion of SVZ accumulated another population of phospho-Vimentin$^+$ progenitors that were Tbr2$^-$ Sox2$^+$ Pax6$^+$ (Fig. 5 *G–G″* and Fig. S5 *A–C*). This progenitor population was relatively small in percentage on day 70 and became prominent by day 91 (Fig. 5*H*). On day 91, this Sox2$^+$ Tbr2$^-$ cell population was biased to localize more basally, in contrast to the apically deviated location of Sox2$^-$ Tbr2$^+$ intermediate progenitors (Fig. 5*I*, *Right*). Interestingly, these two populations responded differently to Notch signal inhibition, which strongly decreases apical progenitors by inducing precocious neuronal differentiation. The Notch inhibitor treatment (days 70–77) increased Sox2$^-$ Tbr2$^+$ intermediate progenitors, whereas Sox2$^+$ Tbr2$^-$ cells rarely remained after the treatment (Fig. S5 *D–F*).

Recent studies have shown that the oSVZ in the human cortex accumulates a Tbr2$^-$ Sox2$^+$ Pax6$^+$ progenitor population distinct from Tbr2$^+$ intermediate progenitors (Fig. S5*G*) (11, 12). These progenitors, termed oRG (or OSVZ progenitors) (11, 12), have a basal process extending to the pial surface and lack an apical process unlike apical progenitors. Similarly, the Tbr2$^-$ Sox2$^+$ Pax6$^+$ progenitors in the day 91 hESC-derived cortical NE also had a basal process but not an apical process (Fig. 5 *J–K′* and Fig. S5 *H*, *H′*, and *I*). These cells had a pericentrin$^+$ basal body in the soma located in the SVZ (Fig. S5*J*), unlike apical progenitors, in which basal bodies are located near the apical surface. Like in vivo oRG, the cleavage plane of the hESC-derived oRG-like cells tended to be horizontal (Fig. 5 *L* and *M*). No basal processes were found in Tbr2$^+$ progenitors (Fig. S5 *K–K″*).

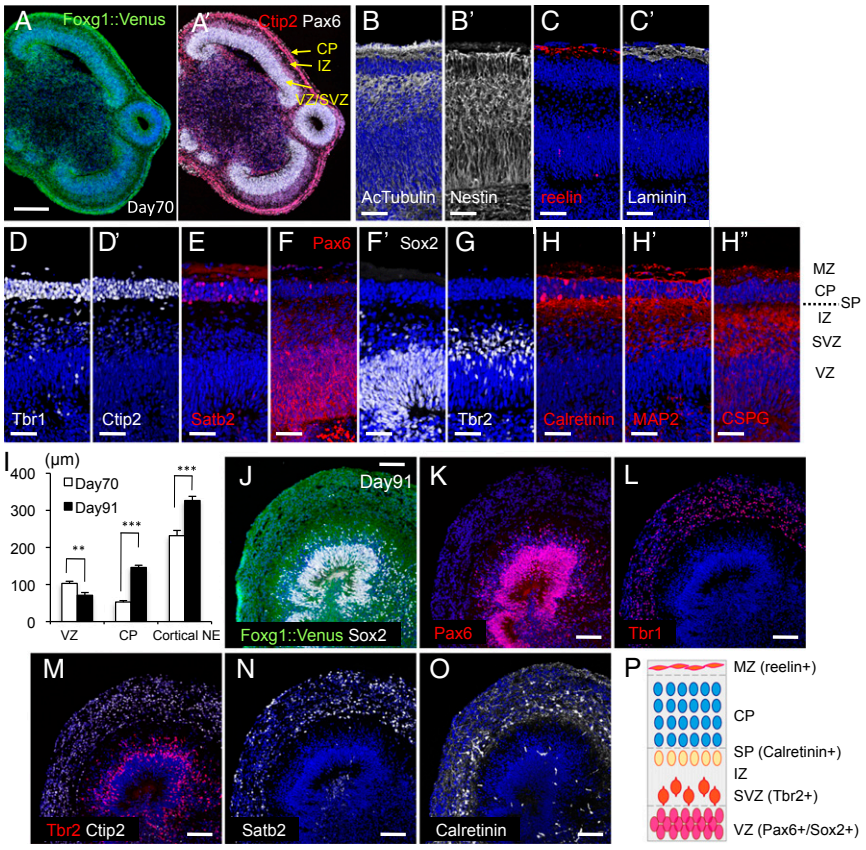

Fig. 3. Self-formation of multiple zones in hESC-derived cortical NE. (*A*) Sections of day 70 hESC-derived cortical NE. Clear separation of VZ (Pax6$^+$), SVZ, intermediate zone, and CP (Ctip2$^+$) was seen even at this low-magnification view. (*B–H*) Immunostaining of day 70 cortical NE with zone-specific markers. (*I*) Total thickness of cortical NE and thickness of ventricular and cortical plate zones on days 70 and 91. $^{**}P < 0.01$; $^{***}P < 0.001$, Student *t* tests between day 70 and day 91 NE samples ($n = 6$, each). (*J–O*) Immunostaining of day 91 cortical NE with zone-specific markers. (*P*) Schematic of the laminar structure seen in long-term culture of hESC-derived cortical NE. (Scale bars, 400 μm in *A*; 50 μm in *B–H″*; 100 μm in *J–O*.) Bars in graph, SEM. Nuclear counter staining (blue), DAPI.

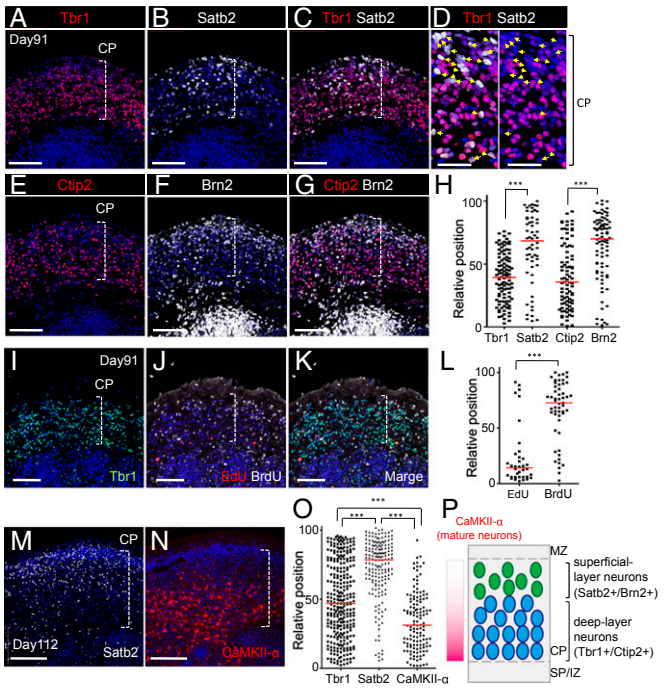

Fig. 4. Basally biased localization of Satb2$^+$ and Brn2$^+$ cortical neurons in CP. (*A–H*) Cortical neurons positive for Satb2 and Brn2 (superficial-layer markers) were preferentially localized to the basal (superficial) portion of the hESC-derived CP in day 91 culture. Most of the basally located Satb2$^+$ cells were negative for the deep-layer marker Tbr1. (*H*) Distribution of marker-positive neurons within the CP. For relative positions, the apical and basal boundaries of the CP were defined as 0 and 100, respectively. ***P < 0.001. Mann-Whitney test. Red line, median. Counted neurons: Tbr1$^+$ (n = 105), Satb2$^+$ (n = 58), Ctip2$^+$ (n = 87), and Brn2$^+$ (n = 86). (*I–L*) Double-pulse labeling study using EdU (day 50; red; n = 36) and BrdU (day 70; white; n = 53). Analyzed by immunostaining on day 91. Statistical analysis was done as in *H*. (*M–O*) The mature cortical neuron marker CaMKII was preferentially expressed in Tbr1$^+$ neurons located in the deep portion of the CP on day 112. The cortical NE was cultured on a Transwell filter during days 78–112 to support robust survival of mature neurons. (*O*) Plotting was done as in *H*. ***P < 0.001. Kruskal-Wallis test with a post hoc multiple comparison test. Numbers of neurons counted: Tbr1$^+$ (n = 293), Satb2$^+$ (n = 177), and CaMKII$^+$ (n = 132). (*P*) Schematic of neuronal distributions within the CP of hESC-derived cortical NE on days 91 and 112. (Scale bars, 100 μm in *A–C*, *E–G*, and *I–K*; 50 μm in *D*; 200 μm in *M* and *N*.) Nuclear counter staining (blue), DAPI.

Discussion

Our optimized culture allowed robust growth of hESC-derived cortical NE in long-term suspension culture, even beyond 13 wk; eventually, the cortical NE became almost 350 μm thick and contained multiple laminar zones as seen in the fetal cortex at the second trimester (starting from embryonic week 11) (30). This robust growth makes a clear contrast to the limitation of our previous 3D culture, which could support the cortical NE development up to the tissue maturation equivalent to the first trimester cortex. The optimized culture also recapitulated another aspect of second-trimester neocorticogenesis, i.e., the appearance of oRG-like progenitors on day 91 (13 wk) of culture. Thus, the developmental speed in our culture is roughly comparable to that in the fetal brain.

The self-organization shown in this study raises many important questions for future investigation. The self-forming mechanism for the intracortical polarity is an intriguing topic, and it would be also interesting to examine whether the frontal lobe-specific characters may appear in the Fgf8-treated aggregate. How the dorsocaudal domain generates a stronger curvature in the rolling morphogenesis is another important question to be addressed using our 3D culture.

Our culture system is also applicable to the study of the dorsal-ventral specification of the whole telencephalic region. Notably, under the partially ventralized conditions (Fig. 2 *O–Q*), the hESC-derived NE recapitulated the continuous self-formation of the cortex and LGE (striatum anlage) in adjacent positions as seen in vivo. The origin of human cortical interneurons may be an intriguing topic to be studied using this system, because they are suggested to arise not only from the subplallium but also from the cortical VZ/SVZ (31, 32) in the human fetus.

The optimized culture allowed the emergence of complex separation of cortical zones. The subplate zone is a particularly predominant structure in the fetal primate cortex (also called layer VII), and consists of early-born neurons within the neocortex (e.g., pioneer neurons) (24, 25). Although this zone is only transiently present in the fetal cortex, some of its derivatives exist in the adult brain as interstitial neurons in the white matter (33). Because the subplate disappears postnatally, its investigation is not easy, especially in humans, and thus, our culture system should be useful in studying this little understood neuronal

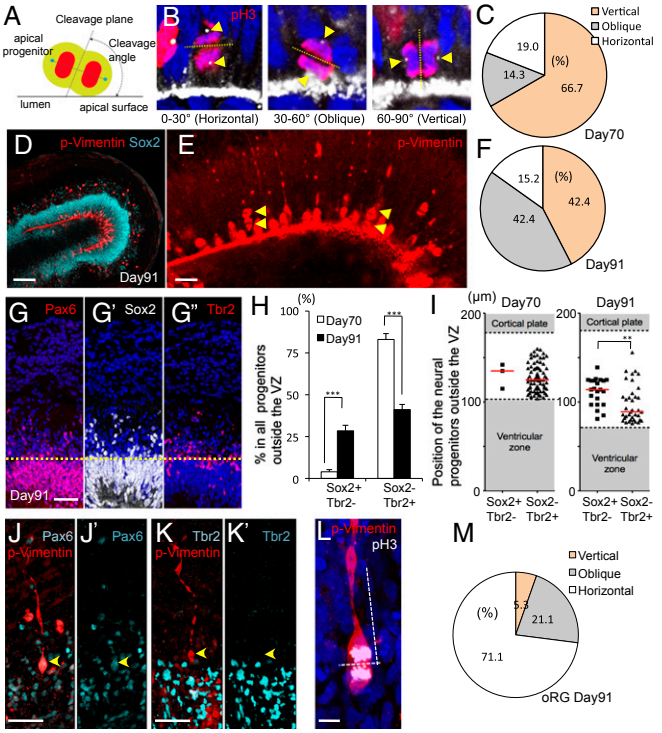

Fig. 5. Appearance of oRG-like progenitors. (*A–F*) Percentages of apical progenitors with vertical (cleavage angle at 60–90°) and nonvertical (0–30° and 30–60°) cleavages (*A* and *B*) in the VZ of day 70 (*C*) and day 91 (*D–F*) hESC-derived cortical NE. p-Vimentin, M-phase marker. Arrowhead, pericentrin. Cells analyzed: n = 42 (day 70) and n = 33 (day 91). (*G–I*) Basal progenitors (Pax6$^+$, Sox2$^+$) and intermediate progenitors (Tbr2$^+$) in the SVZ of day 91 culture. (*H*) Percentages of Sox2$^+$/Tbr2$^-$ and Sox2$^-$/Tbr2$^+$ progenitors within all progenitors (Sox2$^+$ and/or Tbr2$^+$) in the CP. The percentage of Sox2$^+$/Tbr2$^-$ progenitors increased from day 70 to day 91, whereas Sox2$^-$/Tbr2$^+$ progenitors decreased in proportion. ***P < 0.001, Student t tests between day 70 and day 91 samples. Non-VZ progenitors from four cortical NE domains from each day were counted. (*I*) On day 91, Sox2$^+$/Tbr2$^-$ progenitors tended to localize farther from the ventricular surface than Sox2$^-$/Tbr2$^+$ progenitors (*Right*). ***P < 0.001, Mann-Whitney test. Red line, median. (*J–M*) Pax6$^+$ p-Vimentin$^+$ progenitors had a long basal process extending toward the pia but not an apical process (*J* and *J′*), whereas these progenitors were negative for Tbr2 (*K* and *K′*). A majority (>70%) of these SVZ progenitors possessing a basal process showed a horizontal type of cleavage angle (60–90°; *L* and *M*) (n = 37). (Scale bars, 100 μm in *D*; 25 μm in *E*; 50 μm in *G*, *J*, and *K*; 10 μm in *L*.) Bars in graph, SEM. Nuclear counter staining (blue), DAPI.

layer. In addition, our system may be applicable to studies of the inside-out pattern formation in the human fetal cortex, including the pathogenesis of lissencephaly.

Thus far, little has been known about the mechanism of how the cortical NE grows in thickness. One possible mechanism is that the distance between the apical and basal surfaces may be gradually widen by the accumulation of neurons and precursors in the CP and SVZ. However, this idea does not seem to go along with the IZ formation in this self-organizing culture, because this zone is low in cell density and also lacks rigid structural components other than radial glial fibers. Therefore, this zone is difficult to transfer mechanical compression. Our observations suggest that the NE thickness is actively controlled by the growth of the radial glia fiber length.

Finally, our culture should also be very advantageous in studying the role of oRG progenitors in human corticogenesis. It is presumably advantageous for the gyrencephalic human neocortex to involve this type of progenitors that keep on dividing multiple times to generate a number of superficial neurons. To date, there are no specific molecular markers reported for demarcating oRG, and the distinction between oRG and apical progenitors (both are $Sox2^+$, $Pax6^+$, and $Tbr2^-$) mainly depends on their cellular morphology, behavior, and location. Therefore, the extent of oRG study has been fairly limited in the case of dissociation culture that lacks the topological context. In contrast, our system provides a great advantage in this respect, because the 3D context of the developing human cortex can be recapitulated. Very recently, after our submission of this report, an independent study from another group also reported a similar observation of the oRG appearance in the stratified cortical tissue generated from human pluripotent stem cells (34), using a nonselective differentiation method based on only stochastic specification of brain regions (unlike our reproducibly cortex-selective differentiation culture). Of note, their study successfully demonstrated the usefulness of 3D self-organizing culture for studying congenital disorders of brain development such as microcephaly.

A future challenge for the self-organization approach in human corticogenesis study is to recapitulate the morphological separation of all neuronal layers (II/III–VI) within the CP zone, which occurs during the third trimester of human gestation (35).

Materials and Methods

Self-Organized Cortical Generation from hESCs. hESCs were maintained as described previously (16). For cortical NE generation, hESCs were dissociated to single cells and quickly reaggregated using low-cell-adhesion 96-well plates (15) in cortex differentiation medium (9,000 cells per well) containing Glasgow-MEM, 20% Knockout Serum Replacement, and 20 μM Y-27632. IWR1e (Wnt inhibitor) and SB431542 (TGFβ inhibitor) were added to culture to reach 3 and 5 μM, respectively, from day 0 to day 18.

Long-Term Cortical NE Culture. On day 18, the floating aggregates were transferred to a 9-cm Petri dish (non–cell adhesive) and further cultured in suspension using DMEM/F12 medium supplemented with N2 and Chemically Defined Lipid Concentrate under the 40% O_2/5% CO_2 conditions. From day 35, FBS (10% vol/vol), heparin (5 μg/mL), and Matrigel [1% (vol/vol); growth factor–reduced] were also added to the medium. The tissues were cultured using a lumox dish (SARSTEDT; high O_2 penetration) after day 56. From day 70, the concentration of Matrigel was increased [2% (vol/vol)], and B27 supplement (Invitrogen) was also added to the medium.

ACKNOWLEDGMENTS. We thank Keiko Muguruma, Nicholas Love, Momoko Watanabe, and Atsushi Kuwahara for invaluable comments and Jürgen Knoblich for in-depth discussion on his recent study. T.K. is grateful to Seiichi Yokoyama, Yoshiharu Mimamitake, Yasuhiro Kita, Teruyoshi Inoue, and Kumiko Kadoshima for continuous encouragement during this project. This work was supported by grants-in-aid from Ministry of Education, Culture, Sports, Science and Technology (to Y.S. and M.E.), and by the Core Program for Disease Modeling Using iPS Cells (to Y.S.), and the Network Program for Realization of Regenerative Medicine (to Y.S.) from Japan Science and Technology Agency.

1. Molyneaux BJ, Arlotta P, Menezes JR, Macklis JD (2007) Neuronal subtype specification in the cerebral cortex. *Nat Rev Neurosci* 8(6):427–437.
2. Hébert JM, Fishell G (2008) The genetics of early telencephalon patterning: Some assembly required. *Nat Rev Neurosci* 9(9):678–685.
3. Bielle F, et al. (2005) Multiple origins of Cajal-Retzius cells at the borders of the developing pallium. *Nat Neurosci* 8(8):1002–1012.
4. Bystron I, Blakemore C, Rakic P (2008) Development of the human cerebral cortex: Boulder Committee revisited. *Nat Rev Neurosci* 9(2):110–122.
5. Rakic P (1974) Neurons in rhesus monkey visual cortex: Systematic relation between time of origin and eventual disposition. *Science* 183(4123):425–427.
6. Shen Q, et al. (2006) The timing of cortical neurogenesis is encoded within lineages of individual progenitor cells. *Nat Neurosci* 9(6):743–751.
7. Eiraku M, et al. (2008) Self-organized formation of polarized cortical tissues from ESCs and its active manipulation by extrinsic signals. *Cell Stem Cell* 3(5):519–532.
8. Watanabe K, et al. (2005) Directed differentiation of telencephalic precursors from embryonic stem cells. *Nat Neurosci* 8(3):288–296.
9. Nasu M, et al. (2012) Robust formation and maintenance of continuous stratified cortical neuroepithelium by laminin-containing matrix in mouse ES cell culture. *PLoS ONE* 7(12):e53024.
10. Mariani J, et al. (2012) Modeling human cortical development in vitro using induced pluripotent stem cells. *Proc Natl Acad Sci USA* 109(31):12770–12775.
11. Hansen DV, Lui JH, Parker PR, Kriegstein AR (2010) Neurogenic radial glia in the outer subventricular zone of human neocortex. *Nature* 464(7288):554–561.
12. Fietz SA, et al. (2010) OSVZ progenitors of human and ferret neocortex are epithelial-like and expand by integrin signaling. *Nat Neurosci* 13(6):690–699.
13. Wang X, Tsai JW, LaMonica B, Kriegstein AR (2011) A new subtype of progenitor cell in the mouse embryonic neocortex. *Nat Neurosci* 14(5):555–561.
14. Shitamukai A, Konno D, Matsuzaki F (2011) Oblique radial glial divisions in the developing mouse neocortex induce self-renewing progenitors outside the germinal zone that resemble primate outer subventricular zone progenitors. *J Neurosci* 31(10): 3683–3695.
15. Nakano T, et al. (2012) Self-formation of optic cups and storable stratified neural retina from human ESCs. *Cell Stem Cell* 10(6):771–785.
16. Watanabe K, et al. (2007) A ROCK inhibitor permits survival of dissociated human embryonic stem cells. *Nat Biotechnol* 25(6):681–686.
17. Storm EE, et al. (2006) Dose-dependent functions of Fgf8 in regulating telencephalic patterning centers. *Development* 133(9):1831–1844.
18. Fuccillo M, Rallu M, McMahon AP, Fishell G (2004) Temporal requirement for hedgehog signaling in ventral telencephalic patterning. *Development* 131(20): 5031–5040.
19. Danjo T, et al. (2011) Subregional specification of embryonic stem cell-derived ventral telencephalic tissues by timed and combinatory treatment with extrinsic signals. *J Neurosci* 31(5):1919–1933.
20. Yun K, Potter S, Rubenstein JL (2001) Gsh2 and Pax6 play complementary roles in dorsoventral patterning of the mammalian telencephalon. *Development* 128(2): 193–205.
21. Alcamo EA, et al. (2008) Satb2 regulates callosal projection neuron identity in the developing cerebral cortex. *Neuron* 57(3):364–377.
22. Doetsch F (2003) The glial identity of neural stem cells. *Nat Neurosci* 6(11):1127–1134.
23. Kostovic I, Rakic P (1990) Developmental history of the transient subplate zone in the visual and somatosensory cortex of the macaque monkey and human brain. *J Comp Neurol* 297(3):441–470.
24. Wang WZ, et al. (2010) Subplate in the developing cortex of mouse and human. *J Anat* 217(4):368–380.
25. Judaš M, Sedmak G, Kostović I (2013) The significance of the subplate for evolution and developmental plasticity of the human brain. *Front Hum Neurosci* 7:423.
26. Sheppard AM, Pearlman AL (1997) Abnormal reorganization of preplate neurons and their associated extracellular matrix: An early manifestation of altered neocortical development in the reeler mutant mouse. *J Comp Neurol* 378(2):173–179.
27. Bayer SA, Altman J (2005) *Atlas of Human Central Nervous System Development, Volume 3: The Human Brain During the Second Trimester* (CRC Press, Boca Raton, FL).
28. LaMonica BE, Lui JH, Hansen DV, Kriegstein AR (2013) Mitotic spindle orientation predicts outer radial glial cell generation in human neocortex. *Nat Commun* 4:1665.
29. Taverna E, Huttner WB (2010) Neural progenitor nuclei IN motion. *Neuron* 67(6): 906–914.
30. Bayatti N, et al. (2008) A molecular neuroanatomical study of the developing human neocortex from 8 to 17 postconceptional weeks revealing the early differentiation of the subplate and subventricular zone. *Cereb Cortex* 18(7):1536–1548.
31. Letinic K, Zoncu R, Rakic P (2002) Origin of GABAergic neurons in the human neocortex. *Nature* 417(6889):645–649.
32. Rakic S, Zecevic N (2003) Emerging complexity of layer I in human cerebral cortex. *Cereb Cortex* 13(10):1072–1083.
33. Judaš M, Sedmak G, Pletikos M (2010) Early history of subplate and interstitial neurons: From Theodor Meynert (1867) to the discovery of the subplate zone (1974). *J Anat* 217(4):344–367.
34. Lancaster MA, et al. (2013) Cerebral organoids model human brain development and microcephaly. *Nature* 501(7467):373–379.
35. Bayer SA, Altman J (2004) *Atlas of Human Central Nervous System Development, Volume 2: The Human Brain During the Third Trimester* (CRC Press, Boca Raton, FL).

Supporting Information

Kadoshima et al. 10.1073/pnas.1315710110

SI Materials and Methods

Maintenance and Differentiation Culture of hESCs. Human ES cells (hESCs) (KhES-1) were used according to the hESC research guidelines of the Japanese government. hESCs were maintained on a feeder layer of mouse embryonic fibroblast (MEFs) inactivated by mitomycin C treatment in DMEM/F12 (Sigma) supplemented with 20% (vol/vol) Knockout Serum Replacement (KSR; Invitrogen), 2 mM glutamine, 0.1 mM nonessential amino acids (Invitrogen), 5 ng/mL recombinant human basic FGF (Wako), 0.1 mM 2-mercaptoethanol (2-ME), 50 U/mL penicillin, and 50 μg/mL streptomycin under 2% CO_2. For passaging, hESC colonies were detached and recovered en bloc from the feeder layer by treating them with 0.25% (wt/vol) trypsin and 0.1 mg/mL collagenase IV in PBS containing 20% (vol/vol) KSR and 1 mM $CaCl_2$ at 37 °C for 7 min. The detached hESC clumps were broken into smaller pieces (several dozens of cells) by gentle pipetting. The passages were performed at a 1:3–1:4 split ratio.

For serum-free floating culture of embryoid body–like aggregates with quick reaggregation (SFEBq) culture, hESCs were dissociated to single cells in TrypLE Express (Invitrogen) containing 0.05 mg/mL DNase I (Roche) and 10 μM Y-27632, and quickly reaggregated using low-cell-adhesion 96-well plates with V-bottomed conical wells (Sumilon PrimeSurface plate; Sumitomo Bakelite) in cortex differentiation medium (9,000 cells per well, 100 μL) containing 20 μM Y-27632. The cortical differentiation medium was Glasgow-MEM supplemented with 20% (vol/vol) KSR, 0.1 mM nonessential amino acids, 1 mM pyruvate, 0.1 mM 2-mercaptoethanol, 100 U/mL penicillin, and 100 μg/mL streptomycin. Defining the day on which the SFEBq culture was started as day 0, IWR1e (Wnt inhibitor) and SB431542 (TGFβ inhibitor) were added to culture to reach 3 and 5 μM, respectively, from day 0 to day 18.

Cortical neuroepithelium (NE) tissues generated from hESCs were subjected to long-term culture under the following conditions. On day 18, the floating aggregates were transferred from a 96-well plate to a 9-cm Petri dish (noncell adhesive) and further cultured in suspension using DMEM/F12 medium supplemented with N2 (Invitrogen), Chemically Defined Lipid Concentrate (Invitrogen), 0.25 mg/mL Fungizone (GIBCO), 100 U/mL penicillin, and 100 μg/mL streptomycin under 40% O_2/5% CO_2 conditions. From day 35, FBS [final 10% (vol/vol)], heparin (5 μg/mL), and Matrigel [final 1% (vol/vol); growth factor–reduced; BD Biosciences] were also added to the medium. To prevent cell death in the central portions of large aggregates, the aggregates were cut into half-size with fine forceps under a dissecting microscope every 2 wk after day 35 and were cultured using a lumox dish (SARSTEDT; high O_2 penetration) after day 56. From day 70, the concentration of Matrigel was increased [final 2% (vol/vol)] and B27 supplement (Invitrogen) was also added to the medium.

Generation of Knock-In hESC Lines. Our gene-targeting strategy is illustrated in Fig. S2*B* and S3*E*. Site-specific zinc finger nucleases (ZFNs; Sigma-Aldrich) (1) were used to facilitate homologous recombination in hESCs. The ZFNs were designed to cause a double-strand break in exon1 of human *foxg1* and *pax6* genes. To generate the targeting construct, the 5′ arm (2.0 and1.0 kbp, respectively) and 3′ arm (1.0 kbp) were amplified by PCR from KhES-1 genomic DNA. The cDNA of *venus*, encoding a yellow variant of GFP, was fused in-frame into the first exon of *foxg1* and *pax6* genes at the initial *ATG* codon. A *PGK* promoter-driven neomycin-resistance selection cassette flanked by *loxP* sites was inserted downstream of *venus*. For transfection of the targeting vector and ZFN-coding mRNAs, hESCs were dissociated into single cells in TrypLE Express (Invitrogen) containing 0.05 mg/mL DNase I (Roche) and 10 μM Y-27632, and 8×10^5 cells were resuspended in NEON Resuspension Buffer R and electroporated using the Neon transfection system (Invitrogen) with protocol No.17 (850 V, 30 ms, 2 pulses). Transfected cells were plated onto Neo-resistant feeder MEF cells. Homologous-recombinant hESCs selected with 50 μg/mL Geneticin (Gibco) were screened by PCR genotyping.

Immunohistochemistry and FACS. Immunohistochemistry was performed as described (2) with primary antibodies described below. The antibodies were used at the following dilutions: GFP (rat/monoclonal/1:1,000/Nakalai Tesque), aPKC (rabbit/1:100/Santa Cruz), Laminin (rabbit/1:1,000/abcam), Tuj1 (rabbit/1:500/Covance), Ctip2 (rat/1:5,000/abcam), reelin (mouse/1:300/MBL), Sp8 (goat/1:500/Santa Cruz), Phospho-MLC2 (rabbit/1:500/CST), Nkx2.1 (mouse/1:500/Novocastra), GAD65 (mouse/1:200/Becton Dickinson), Nestin (rabbit/1:200/Covance), Satb2 (mouse/1:75/abcam), MAP2 (mouse/1:200/Sigma), CSPG (mouse/1:200/Sigma), Brn2 (goat/1:300/Santa Cruz), CaMKII (mouse/1:500/abcam) or (rabbit/1:100/Santa Cruz), Pericentrin (rabbit/1:2,000/abcam), phospho-vimentin-Ser55 (mouse/1:500/abcam), Sox2 (goat/1:250/Santa Cruz), Acetylated-α-Tubulin (mouse/1:500/Abcam), *N*-cadherin (mouse/1:1,000/Becton Dickinson), Calretinin (rabbit/1:2,000/Chemicon), phospho-Histone H3-Ser10 (mouse/1:500/CST) or (rabbit/1:1,500/CST), Foxg1 (rabbit/1:1,000) (3), Gsh2 (rabbit/1:10000) (3), Pax6 (rabbit/1:250/Covance), Tbr2 (rabbit/1:500/abcam), Tbr1 (rabbit/1:500/abcam), CoupTF-1 (mouse/1:1,000/Preseus), Lhx2 (goat/1:100/Santa Cruz) and Otx2 (rabbit/1:1,000/abcam), TAG1 (mouse/1:200/DSHB), and phospho-Erk (rabbit/1:200/CST). The antiserum against Zic1 was raised in rabbits against a synthetic peptide (AVHHTAGHSALSSNFNEC; corresponding to the C-terminal residues 428–444 of the human Zic1 protein) and was affinity purified (1:20,000). The antiserum against Lmx1a was raised in guinea pigs against a synthetic peptide (CFLATSEAGPLQSRVGNPIDHLYSMQNSYFTS; corresponding to the C-terminal residues 351–382 of the human Lmx1a protein) and was affinity purified (1:20,000). To detect the nuclear incorporation of BrdU and EdU, we used a BrdU antibody (mouse/1:50/BD) and the Click-iT EdU Imaging Kit (Invitrogen) with an antigen retrieval procedure (S1699/DAKO). Expression patterns of the following markers in the embryonic brain are described in refs. 4–9: Pax6, Tbr2, Tbr1, CoupTF-1, Lhx2, Zic1, and Lmx1a. Counter nuclear staining was performed with DAPI (Molecular Probes). To observe outer radial glia (oRG)-like cells, we performed vibratome section staining and whole-mount staining of SFEBq aggregates. For vibratome section staining, fixed aggregates were embedded in 4% low-melting agarose in PBS, cut at 300 μm. Floating vibratome sections and aggregates were permeabilized (0.3% Triton X-100 in PBS, 1 h, room temperature) and blocked overnight with 2% (wt/vol) skim milk and 0.1% Tween-20 in Tris-buffered saline (TBS) at 4 °C. Specimens were incubated with primary antibodies for 2 d at 4 °C and washed with 0.1% Tween-20 in TBS three times for 1 h each, followed by incubation with secondary antibody overnight at 4 °C. After being washed, specimens were incubated in clearing solution (ScaleA2 or benzyl alcohol/benzyl benzoate) and imaged with a confocal microscope (LSM710; Carl Zeiss).

For FACS analysis, cells (from 48 aggregates per experiment) were dissociated to single cells using a Nerve-Cell Dissociation media Kit (Sumitomo Bakelite), analyzed at 4 °C, and counted

with FACSAria (Becton Dickinson). The data were analyzed with FACSDiva software (Becton Dickinson).

Live Imaging of Cortical NE. Three-dimensional live imaging was performed as described (10) using specially assembled inverted multiphoton microscopes (based on Olympus FV-1000/MPE) combined with a full-sized CO_2/O_2 incubator. The position of the ESC aggregate was fixed in a drop of undiluted Matrigel, which was then immersed in culture medium (described above) on a 3.5-cm glass-bottom dish (Movie S1). For high-resolution multiphoton live imaging, a stack of optical section images (512 × 512 pixels for the *X*–*Y* plane and 2 μm for *Z* axis step; typically 150 sections) was captured at each time point using a 25× water-immersion lens (N.A. 1.05; Olympus) and multiphoton femtosecond laser (920 nm; Mai-Tai DeepSee eHP; Spectra-Physics) with group velocity dispersion autocompensation. The 3D image analyses were done with Imaris 7.6 (Bitplane). The bright-field view in parallel to multiphoton imaging was obtained by scanning with a 920-nm femtosecond laser and detecting the transmission light with a separate photo-multiplier.

Quantifications and Statistical Analysis. Statistical tests were performed with PRISM software (GraphPad, ver 5). Statistical significance was tested with the Student *t* test (parametric) or Mann-Whitney test (nonparametric) for two-group comparison or with the Dunnett test (parameteric; vs. the control group) or the Kruskal-Wallis ANOVA test by ranks (nonparametric) for multiple-group comparison. Nonparametric analyses were applied to the analyses of tissue distribution of neurons and progenitors in Figs. 4 and 5, because their distribution patterns did not appear to be Gaussian. For Fig. 3*I*, there was no need for no comparison among three aspects of thickness (VZ, CP, and cortical NE), whereas their measurement and comparison on these 2 d had been planned a priori. Therefore, their statistical analyses were done individually as three independent studies with *t* tests, rather than applying a two-way ANOVA test. The same rationale for choosing the statistical test was applied to the *t* tests in Fig. 5*H*. Contingency table (2 × 2) analysis was tested with Fisher's exact test.

For the rostralization of neocortical NE, aggregates were treated with recombinant human FGF8b (200 ng/mL; Gibco) during days 24–42. On day 42, the aggregates were fixed and cryosectioned. Sections were immunostained with CoupTF-1 and Sp8 antibody, and the percentages of CoupTF-1$^+$ and Sp8$^+$ VZ in the neocortical VZ were quantified. To examine the effects of the Rho kinase (ROCK) inhibitor on the rolling morphogenesis of neocortical NE, aggregates were treated with the ROCK inhibitor Y-27632 (10 μM) during days 26–30. On day 30, the aggregates were fixed and cryosectioned. Sections were immunostained with acetylated-α-tubulin antibody, and the percentage of NE with or without rolling morphogenesis was quantified.

For the ventralization of neocortical NE, aggregates were treated with Hedgehog agonist [smoothened agonist (SAG)] (30 or 500 nM) during days 15–21. On day 35, the aggregates were fixed and cryosectioned. Sections were immunostained with GFP, Pax6, and Gsh2 antibody. For quantification of the regional marker expression in aggregates, the percentages of Foxg1$^+$/Pax6$^+$ NE and Foxg1$^+$/Gsh2$^+$ NE in each aggregate were calculated as the sum of angular degrees of each type of NE from the aggregate center using Image J and presented as percentages. The thickness of VZ, cortical plate, and cortical NE, and the distance from the ventricular surface of neural progenitors, were determined by tracing them using Image J. For the quantification of the cleavage plane orientation of apical progenitors, sections of day 70 and day 91 aggregates were immunostained with phospho-histone H3 and Pericentrin antibody. We examined the cleavage plane orientations of anaphase and telophase cells, which were close to the ventricular surface, with a cleavage plane parallel to the ventricular surface being defined as 0°. For the quantification of the cleavage plane orientation of oRG-like cells, vibratome sections of day 91 aggregates were immunostained with phospho-vimentin and phospho-histone H3 antibody. We examined the cleavage plane orientations of anaphase and telophase cells outside the VZ that had a basal process, with a cleavage plane parallel to the basal process being defined as 0°.

1. Porteus M (2008) Design and testing of zinc finger nucleases for use in mammalian cells. *Methods Mol Biol* 435:47–61.
2. Eiraku M, et al. (2008) Self-organized formation of polarized cortical tissues from ESCs and its active manipulation by extrinsic signals. *Cell Stem Cell* 3(5):519–532.
3. Watanabe K, et al. (2005) Directed differentiation of telencephalic precursors from embryonic stem cells. *Nat Neurosci* 8(3):288–296.
4. Englund C, et al. (2005) Pax6, Tbr2, and Tbr1 are expressed sequentially by radial glia, intermediate progenitor cells, and postmitotic neurons in developing neocortex. *J Neurosci* 25(1):247–251.
5. Zhou C, Tsai SY, Tsai MJ (2001) COUP-TFI: an intrinsic factor for early regionalization of the neocortex. *Genes Dev* 15(16):2054–2059.
6. Mangale VS, et al. (2008) Lhx2 selector activity specifies cortical identity and suppresses hippocampal organizer fate. *Science* 319(5861):304–309.
7. von Frowein J, Wizenmann A, Götz M (2006) The transcription factors Emx1 and Emx2 suppress choroid plexus development and promote neuroepithelial cell fate. *Dev Biol* 296(1):239–252.
8. Inoue T, Ota M, Ogawa M, Mikoshiba K, Aruga J (2007) Zic1 and Zic3 regulate medial forebrain development through expansion of neuronal progenitors. *J Neurosci* 27(20):5461–5473.
9. Failli V, Bachy I, Rétaux S (2002) Expression of the LIM-homeodomain gene Lmx1a (dreher) during development of the mouse nervous system. *Mech Dev* 118(1-2): 225–228.
10. Eiraku M, et al. (2011) Self-organizing optic-cup morphogenesis in three-dimensional culture. *Nature* 472(7341):51–56.

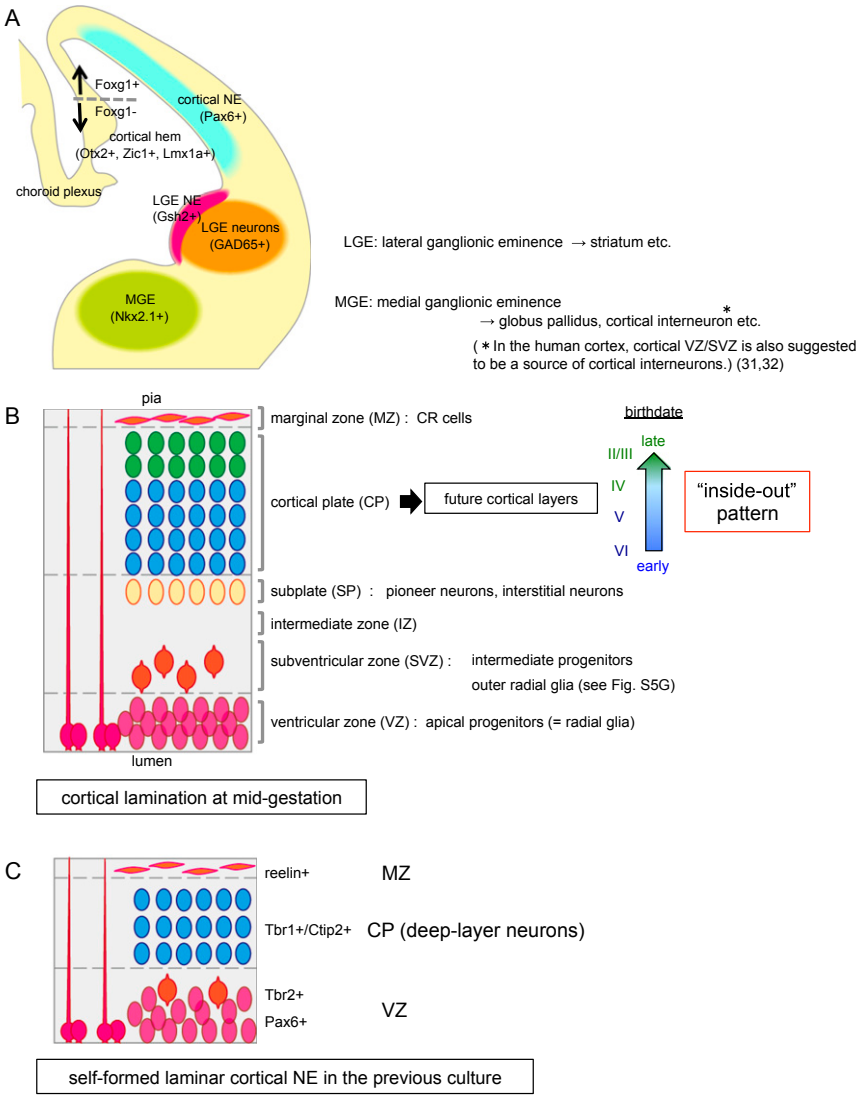

Fig. S1. Development of fetal cortical NE. (*A*) Schematic of the developing fetal telencephalon. (*B*) Schematic of the stratified structure of fetal cortical NE at the early second trimester of human gestation (approximately embryonic week 13). (*C*) Schematic of the laminar cortical NE structure generated in our previous self-organizing culture of hESCs. The structure is similar to the human cortical architecture during the early trimester.

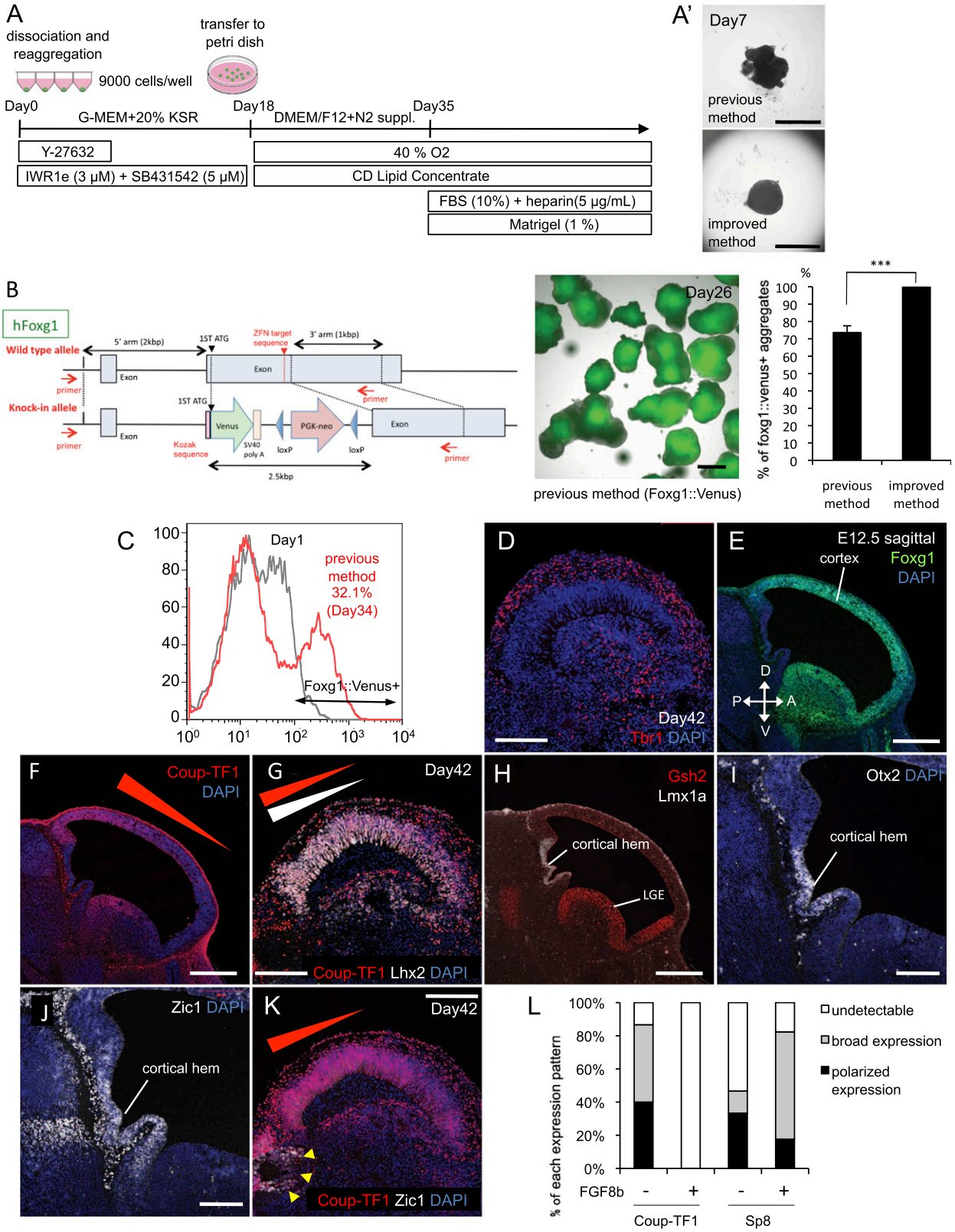

Fig. S2. Axial polarity in hESC-derived cortical NE. (*A*) Schematic of improved culture procedures. (*A'*) Comparison of aggregate formation of hESCs on day 7. (*Upper*) Our previous culture; (*Lower*) the improved culture, which promoted the formation of undivided, smooth aggregates from dissociated hESCs. (*B*) Percentages of hESC aggregates (day 26) that contained NE with substantial *foxg1*::Venus signals. ***$P < 0.001$, Student *t* tests. The knock-in vector construction is shown (*Left*). (*C*) Representative FACS analysis for *foxg1*::Venus^{+} populations. Gray, control (day 1 culture); red, day 34 culture under the previous conditions. (*D*) Immunostaining signals of Tbr1 in the CP of day 42 cortical NE. (*E* and *F*) Localization of regional markers in the mouse fetal telencephalon (Foxg1^{+}; *E*). Coup-TF1 expression in the cortical NE is strong in the dorsocaudal region but weak in the ventrorostral region (*F*). (*G*) Double immunostaining of

Legend continued on following page

CoupTF1 and Lhx2 showed that their expression patterns were similarly biased. (*H–J*) Parasagittal sections of the mouse telencephalon at E12.5. Gsh2, LGE (lateral ganglionic eminence) marker (*H*); Lmx1a, cortical hem and choroid plexus marker (*I*); Otx2 and Zic1, cortical hem markers (*I* and *J*). (*K*) Double immunostaining of Coup-TF1 and Zic1 showed that the cortical hem marker Zic1 was expressed in the tissue flanking the cortical NE on the side with strong Coup-TF1 expression. (*L*) Effects of Fgf8 treatment (days 24–42) on the expression of CoupTF1 and Sp8. Percentages of polarized expression (black), board expression (gray), and undetectable signals (open) were counted in the cross sections (at the longest-axis position) of cortical NE. Because it was counted in this manner, the percentages of polarized expression patterns could be somewhat underestimated. (Scale bars, 1 mm in *A′* and *B*; 200 μm in *D, G,* and *I–K*; 500 μm in *E, F,* and *H*.) Bars in graph, SEM.

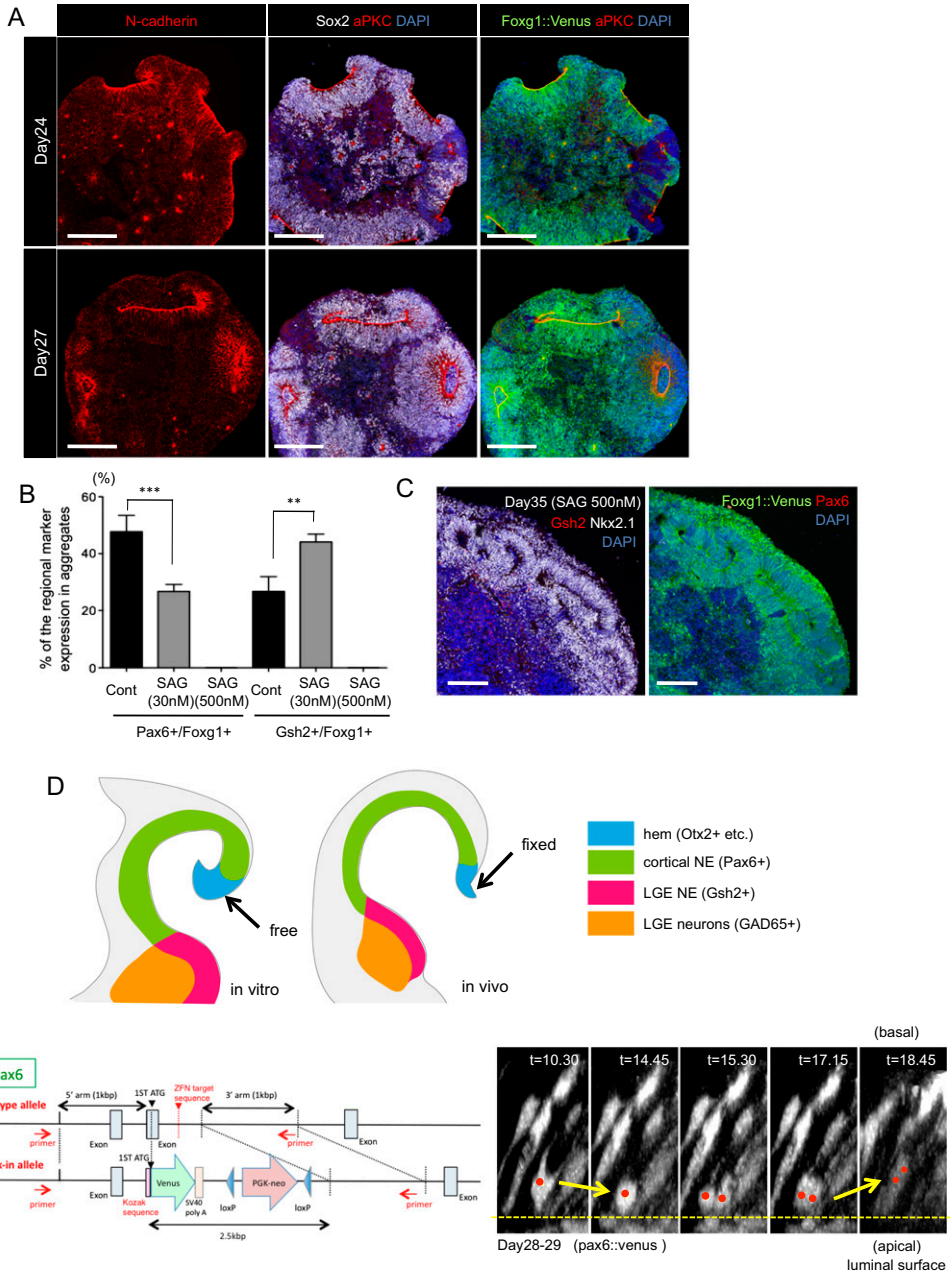

Fig. S3. Rounding morphogenesis and apical division in cortical NE. (*A*) Spontaneous rounding morphogenesis of cortical NE domains in hESC aggregates: (*Upper*) day 24; (*Lower*) day 27. aPKC, apical marker. (*B*) Percentages of $Pax6^+$ (cortical) and $Gsh2^+$ (lateral ganglionic eminence) NE in $Foxg1^+$ telencephalic NE derived from hESCs. Treatment with a moderate concentration of SAG (30 nM; days 15–21; gray columns) partially suppressed the percentage of $Pax6^+$ NE and increased that of $Gsh2^+$ NE. Under this condition, relatively large domains of $Pax6^+$ NE and $Gsh2^+$ NE were frequently found side by side. At 500 nM, SAG treatment efficiently suppressed the expression of both Pax6 and Gsh2. $^{**}P < 0.01$ and $^{***}P < 0.001$, Dunnett's test. (*C*) Expression of the medial ganglionic eminence marker Nkx2.1 in cortical NE treated with 500 nM SAG. $Nkx2.1^+$ NE typically occupied 40–50% of $Foxg1^+$ telencephalic NE. (*D*) Schematic of cortical morphogenesis in hESC culture in comparison with the fetal cortex. (*E*) Symmetrical divisions of apical progenitors near the luminal (apical) surface on days 28–29, whch approached the luminal surface before their cell divisions with a vertical cleavage angle (see Fig. 5 for definition) and moved basally together. Visualized by *pax6::venus* hESCs (partial mixing with WT hESCs). The knock-in vector construction is shown (*Left*). (Scale bars, 200 μm in *A* and *C*.) Bars in graph, SEM.

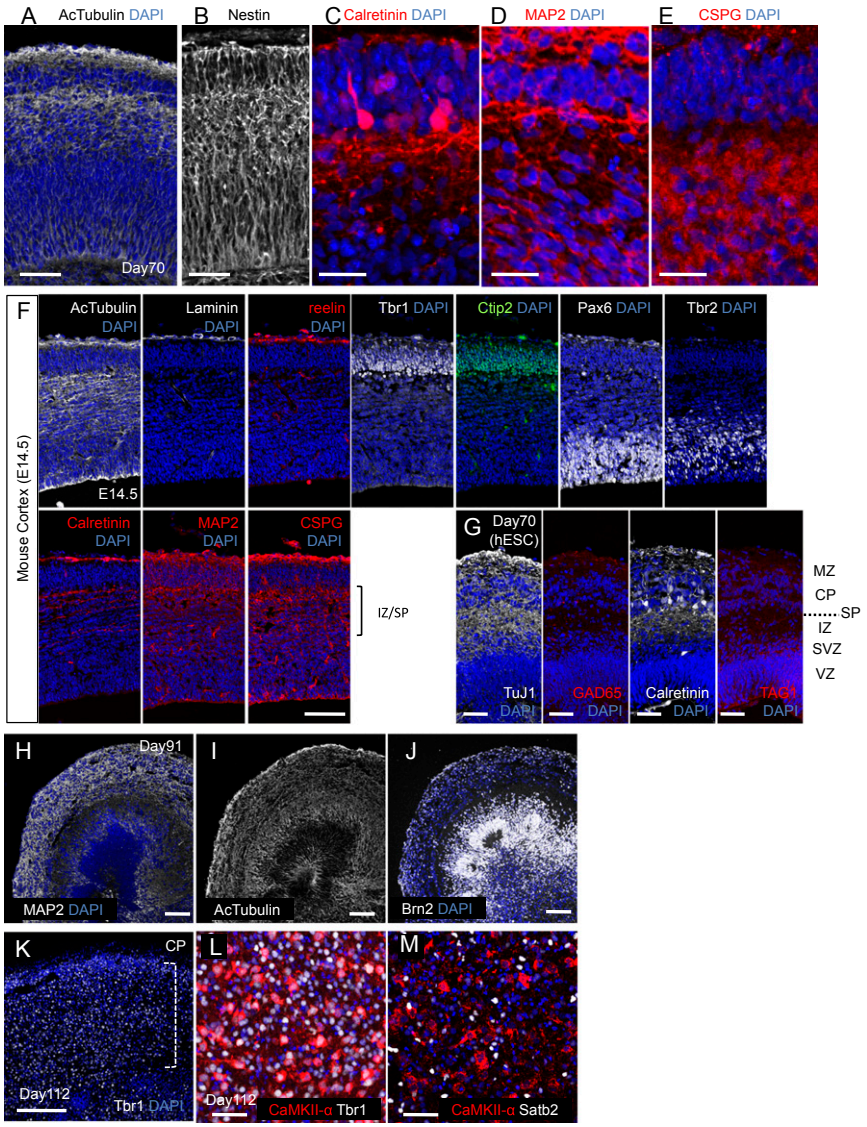

Fig. S4. Subplate formation in hESC-derived cortical NE. (*A–E*) Immunostaining of day 70 hESC-derived cortical NE. (*A* and *B*) Clear morphological zone separations were observed in the cortical NE even by simple staining with acetylated tubulin (AcTubulin; stabilized microtubules), DAPI (nuclear staining), and Nestin (intermediate filaments of neural progenitors). (*C–E*) High-magnification views of calretinin$^+$ neurons (*C*), MAP2$^+$ early neurites (*D*), and CSPG accumulation in the intermediate zone (*E*) of the cortical NE. (*F*) Immunostaning of zone markers in the E14.5 mouse fetal cortex. (*G*) Immunostaining of day 70 hESC-derived cortical NE. No substantial accumulation of GAD65$^+$ interneurons in the CP or TAG1$^+$ corticofugal axons was observed. (*H–J*) Immunostaining of day 91 hESC-derived cortical NE. The cortical NE developed well and the stratified structure became much thicker (*H* and *I*). The CP contained a number of Brn2$^+$ superficial-layer neurons (*J*). (*K*) Immunostaining signals of Tbr1 in the CP of day 112 hESC-derived cortical NE. (*L* and *M*) Expression of the mature cortical neuron marker CaMKIIα in CP of day 112 hESC-derived cortical NE. The majority of these CaMKII neurons coexpressed Tbr1 (*L*) but not Satb2 (*M*). (Scale bars, 50 μm in *A, B, G, L,* and *M*; 20 μm in *C–E*; 100 μm in *F* and *H–J*; 200 μm in *K*.)

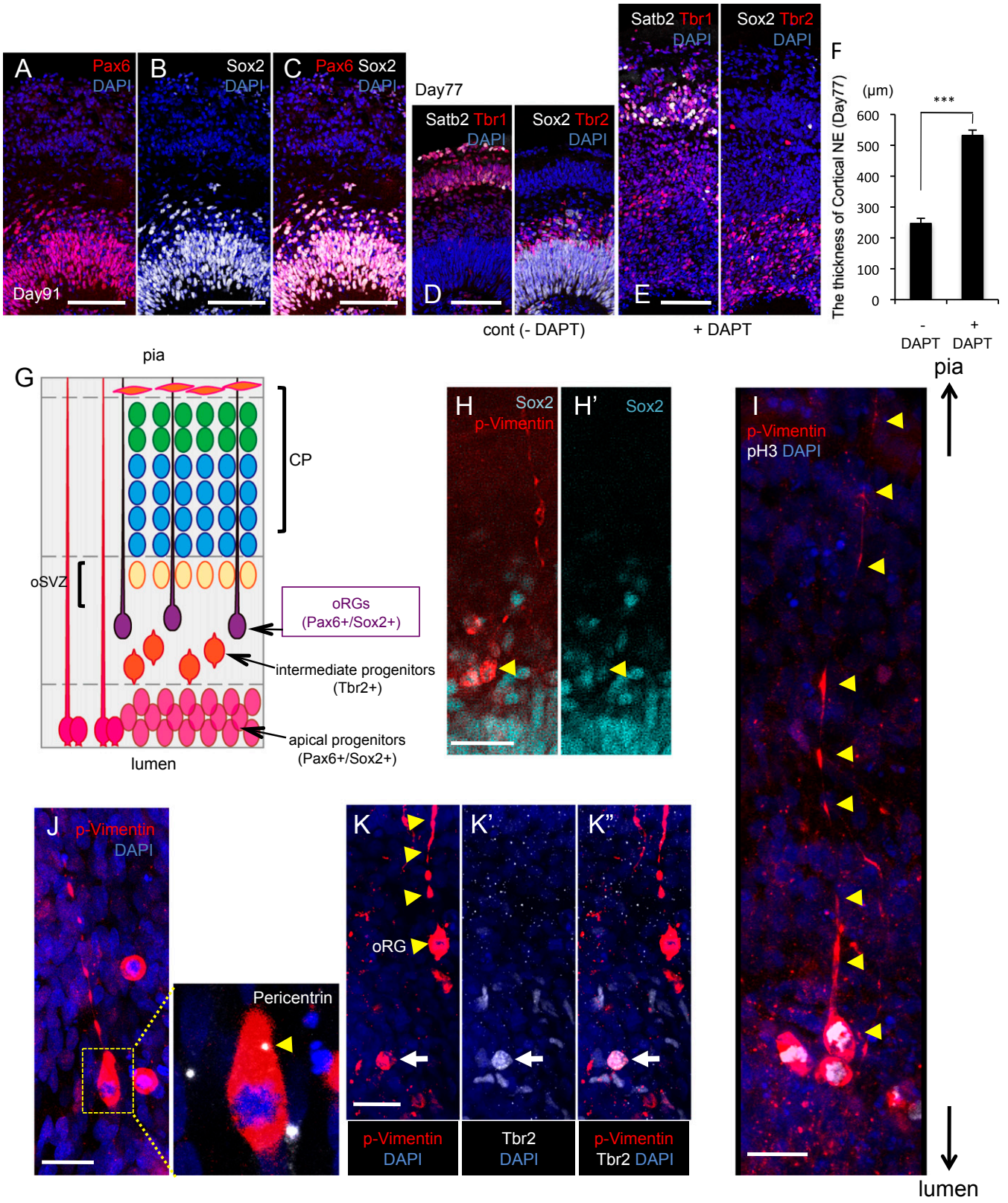

Fig. S5. oRG-like progenitors in the oSVZ. (*A–C*) Immunostaining of Pax6 and Sox2 in apical and basal (SVZ) progenitors within the hESC-derived cortical NE on day 91. The majority of Sox2 signals colocalized with Pax6 signals (*C*). (*D–F*) Effects of Notch signal inhibition on the expression of progenitor and neuron markers in cortical NE. The Notch inhibitor treatment (10 μM DAPT, days 70–77) increased $Sox2^{-}$ $Tbr2^{+}$ intermediate progenitors, whereas $Sox2^{+}$ $Tbr2^{-}$ cells rarely remained after the treatment (*D* and *E*). $Satb2^{+}$ neurons also increased by DAPT treatment (*D* and *E*). A substantial increase of cortical NE thickness also observed after the treatment (*F*). $***P < 0.001$, Student *t* tests between with DAPT ($n = 6$) and without DAPT ($n = 5$) treatment. (*G*) Schematic of oRG in the human fetal outer SVZ. (*H* and *H'*) Phospho-vimentin^{+} progenitors in the SVZ expressed Sox2. (*I*) Phospho-vimentin^{+} progenitors in the SVZ with a long apical

Legend continued on following page

process extending toward the pial surface (no apical process). (*J*) Phospho-vimentin$^+$ SVZ progenitors with a basal process carried a pericentin$^+$ basal body in the soma. During mitosis, two pericentin$^+$ centrioles were found for dividing cells. (*K*–*K*″) Unlike oRG-like progenitors, no Tbr2$^+$ phospho-vimentin$^+$ progenitors in the hESC-derived cortical NE possessed a basal process (nor an apical process). (Scale bars, 100 μm in *A*–*E*; 25 μm in *H*–*K*.)

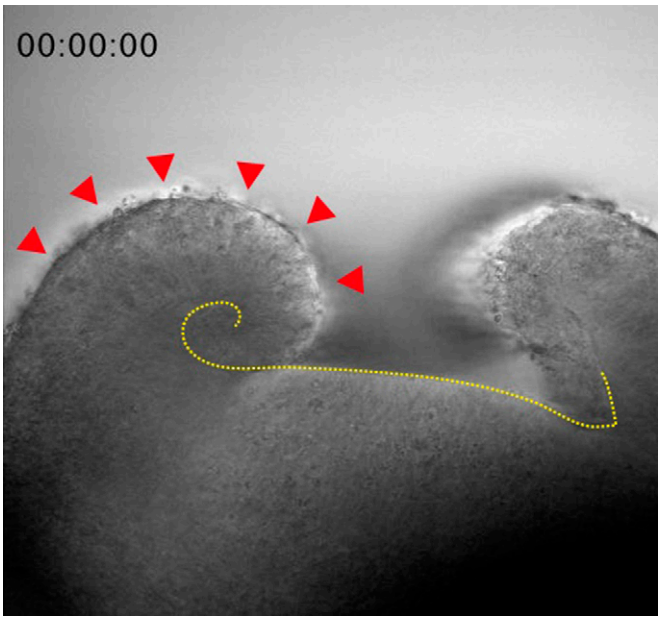

Movie S1. Rounding morphogenesis of hESC-derived cortical NE. Bright field view taken by multiphoton optics during days 24.5–27.

Movie S1

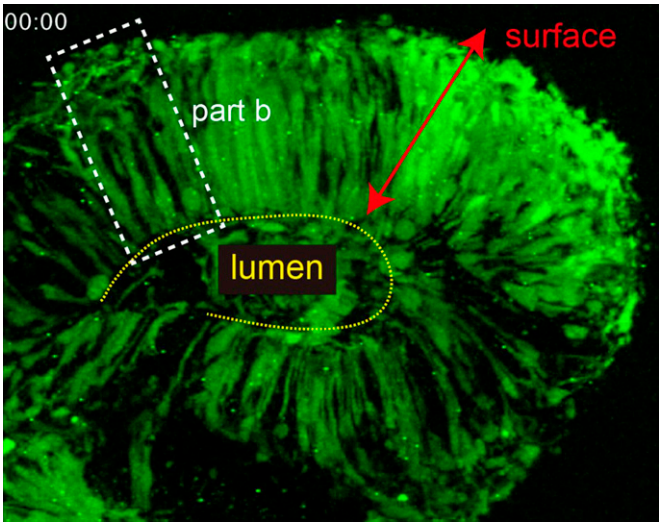

Movie S2. Interkinetic nuclear migration in hESC-derived cortical NE. Live imaging of progenitors (days 24–25) with multiphoton microscopy. Cell morphology was visualized with partial mixing of *pax6::venus* hESCs with nonlabeled hESCs. (*A*) Low-magnification view. (*B*) High-magnification view for an apical progenitor undergoing symmetrical division and generating two daughter progenitors that possess both apical and basal processes.

Movie S2

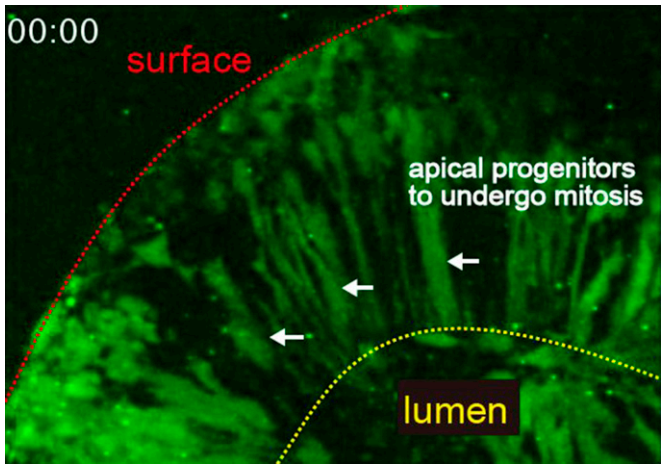

Movie S3. Interkinetic nuclear migration in hESC-derived apical progenitors. High-magnification view of apical progenitors undergoing mitosis.

Movie S3